Unified intermediate coupling description of pseudogap and strange metal phases of cuprates

H. C. Kao,[1,*] Dingping Li,[2,3,†] and Baruch Rosenstein[4,‡]
[1]*Physics Department, National Taiwan Normal University, Taipei 11677, Taiwan, Republic of China*
[2]*School of Physics, Peking University, Beijing 100871, China*
[3]*Collaborative Innovation Center of Quantum Matter, Beijing, China*
[4]*Electrophysics Department, National Chiao Tung University, Hsinchu 30050, Taiwan, Republic of China*

(Received 29 September 2021; revised 11 February 2023; accepted 13 February 2023; published 24 February 2023)

A one band Hubbard model with intermediate coupling is shown to describe the two most important unusual features of a normal state: linear resistivity strange metal and the pseudogap. Both the spectroscopic and transport properties of the cuprates are considered on the same footing by employing a relatively simple post-Gaussian approximation valid for the intermediate couplings $U/t = 1.5$–4 in relevant temperatures $T > 100$ K. In the doping range $p = 0.1$–0.3, the value of U is smaller than that in the parent material. For a smaller doping, especially in the Mott insulator phase, the coupling is large compared to the effective tight binding scale and a different method is required. This scenario provides an alternative to the paradigm that the coupling should be strong, say $U/t > 6$, in order to describe the strange metal. We argue that, to obtain phenomenologically acceptable underdoped normal state characteristics like T^*, pseudogap values, and spectral weight distribution, a large value of U is detrimental. Surprisingly the resistivity in the above temperature range is linear, $\rho = \rho_0 + \alpha \frac{m^*}{e^2 n\hbar} T$, with the "Planckian" coefficient α of order 1.

DOI: 10.1103/PhysRevB.107.054508

I. INTRODUCTION

The physical nature of the d-wave pairing in high-T_c cuprates remains a hotly debated topic in condensed matter physics. However, it was noticed early on that the normal state is as unusual as the superconducting one. The two main unusual features, broadly referred to as the pseudogap [1] and the strange metal [2], cannot be described in the customary framework of the Landau liquid. A pseudogap appears near the antinodal points below temperature T^* and increases in the underdoped regime $p < p_{\rm opt}$ ($p_{\rm opt} = 0.16$) towards the Mott insulator phase, reaching values $\Delta = 100$–200 meV [3,4]. A natural explanation relies on the short range antiferromagnetic (AF) order, since the pseudogap regime borders the Mott insulator phase at very low doping. It was observed [5] that the Fermi surface fractures into small "pockets" for doping below the Lifshitz point p^* precisely when the pseudogap vanishes. This is described quite well by variants of the phenomenological resonating valence bond (RVB) model [6] derived from a Hubbard model with on site repulsion U (and various hopping parameters $t, t', \ldots$) within a generalization of the mean field theory largely preserving the quasiparticle picture [7].

The hallmark of the strange metal is linear resistivity in the 100–450 K temperature range at intermediate and relatively large doping, generally above T^*. It is believed that the quasiparticle picture should be properly modified in this phase. Approaches like the marginal Fermi liquid [8], quantum criticality [9], and Planckian dissipation [10], explain part of the experimental results, but typically start from Hamiltonians different from those used to describe the pseudogap physics. Thus each particular aspect of the normal state can be captured by a particular phenomenological model to provide a consistent description of the whole normal state (not including superconductivity) phase diagram (see Fig. 3), but a single theory is still a challenge. The main problem seems to be the conflict between two "paradigms." It is widely accepted that *strong* electron correlations (in our case on-site repulsion U larger than the band width of $\sim 5t$) play a central role in both the spin fluctuation theory of the d-wave superconductivity and in the normal state properties. It seems consistent with the measured values of $U \sim 1$–3 eV for the parent material ($x = 0$) Mott gap in many cuprates. First-principles derivations (almost exclusively at zero doping) of the "mesoscopic" one-band Hamiltonian support a strong coupling [11]. For one-layer cuprates, one obtains $U = 7.7t$ for La_2CuO_4 ($T_c = 34$ K at $p_{\rm opt}$) and $U = 7.2t$ for $HgBa_2CuO_4$ ($T_c = 96$ K). The trend upon the inclusion of the long range Coulomb interactions on the microscopic level, however, is towards lower values [12]: $U = 6.6t$ for La_2CuO_4 and $U = 4.5t$ for $HgBa_2CuO_4$. Electron doped and infinite layer cuprates have significantly lower values $U/t = 1.3$–3, so that in some cases the Mott insulator phase is missing [13], e.g., for Nd_2CuO_4 ($T_c = 24$ K) one obtains [12] $U/t = 2.6$.

Upon doping, the effective coupling strength U in the mesoscopic level is expected to decrease. Recently a first-principles study of doped cuprates $La_{2-p}Sr_pCuO_4$, $p = 0.25$, was performed [14]. Although the values of U were not explicitly calculated, reduction of the gap at the crystallographic X point by a factor of 2.5 compared to the parent material

*hckao@phy.ntnu.edu.tw
†lidp@pku.edu.cn
‡baruchro@hotmail.com

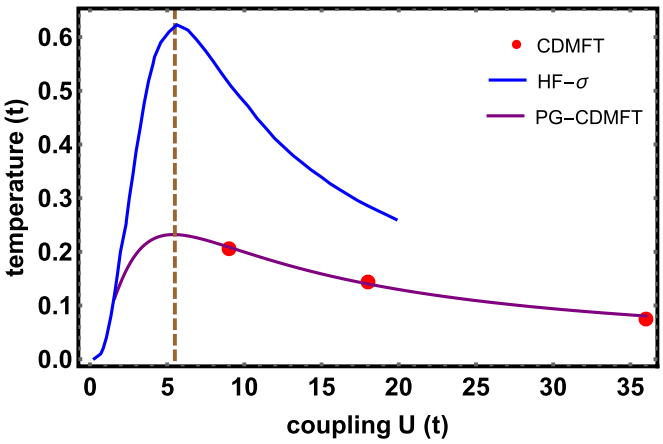

FIG. 1. The crossover temperature T^* in the Hubbard model with ($t' = 0$) at half filling. The blue curve is the HF approximation at small coupling and the nonlinear σ model at large coupling interpolation. The purple curve is the Gaussian perturbation theory at intermediate coupling interpolated with the CDMFT diagrammatic approach at strong coupling.

indicates a lower value. To graphically demonstrate the qualitative distinction between the strongly and intermediate coupling regimes, let us look at the crossover temperature T^* in the simplest Hubbard model at half filling. Interpolating between the early "simplistic" Hartree-Fock (HF) approximation at small coupling and the nonlinear σ model at large coupling [15], one expects a maximum to appear at $U = 5t$, (blue curve in Fig. 1). The Gaussian perturbation theory at intermediate coupling (described below; see also [16]) interpolated with the cluster dynamical mean-field theory (CDMFT) diagrammatic approach [17] at strong coupling gives rise to a correction (purple curve in Fig. 1). The U dependences of T^* obtained from these two calculations share the same feature: rising monotonically at intermediate coupling and decreasing at strong coupling. This separates the (Slater) weakly correlated domain from the (Mott-Heisenberg) strongly correlated domain. It is sometimes referred to [12,18] as the "Mott-Slater transition." The feature remains intact (with typically lower values of T^*) at nonzero doping.

The high values of the coupling at optimal doping are naturally favored in the Hubbard model description of both the normal and superconducting states. Recently, however, serious doubts were cast on this possibility. Employing the tensor network [19], constrained path quantum Monte Carlo (CPQMC), density matrix renormalization group (DMRG) [20], and the strong coupling diagram technique (SCDT) [21] methods, it was demonstrated that the d-wave superconductivity is superseded by other phases at least for $U > 6t$. In the Slater regime the Hubbard model does exhibit d-wave superconductivity within perturbation theory [22], but its T_c is too low. Whether the Hubbard model supports sufficiently strong d-wave superconductivity in the intermediate region $2 < U/t < 5$ is still an open question considering recent opposite claims [23,24]. In addition the coupling strength is poorly correlated with the observed values in cuprates, e.g., the highest $T_c = 133$ K (under ambient conditions) trilayer superconductor [12] $HgBa_2Ca_2Cu_3O_8$ has a density-functional theory (DFT) estimated (zero doping) value of $U/t = 2.5$ only. To quote the authors, "Our results suggest that the strong correlation enough to induce Mott gap may not be a prerequisite for the high- T_c superconductivity." Recent alternatives include the apical phonon [24] and polaron [25] mechanisms.

A general feature of the strong coupling scenario is that the spectrum is expected to be greatly reconstructed and might not contain well defined quasiparticles. However, quasiparticles are observed in numerous experiments, perhaps excluding the strange metal regions [26]. Angle-resolved photoemission spectroscopy (ARPES) experiments and transport properties are "phenomenologically" described by the quasiparticle picture, thus tacitly assuming a weak coupling. This includes description of small Fermi "pockets" in the underdoped regime, and the Landau liquid in highly overdoped samples [6]. In addition the order of magnitude of the pseudogap (up to 200 meV at $p = 0.05$) is smaller than U for strong coupling, thus favoring an intermediate coupling option $U/t \sim 2$–4. In this case the quasiparticles are well defined and the symmetrized mean field approach [16] may be used to describe the temperature range above 100 K and doping above $p = 0.1$. This includes physics of the strange metal and pseudogap for sufficiently large Fermi arcs (pockets).

In this paper the normal state properties of a generic (one layer) hole cuprate (e.g. $HgBa_2CuO_{4+p}$) in the doping range $0.1 < p < 0.3$ and temperature range $100 < T < 460$ K are described by the one-band intermediate coupling Hubbard model. The symmetrization method [16] describing the short range AF state $T < T^*$ is applied to calculate both the spectral weight and conductivity. Surprisingly, linear resistivity, $\rho = \rho_0 + AT$, is obtained with A comparing well with experiments [10,27]. Quantitative comparison of the conductivity with experiments therefore goes beyond scaling arguments [9]. The transition at T^* is comparable to that observed in ARPES [28] or transport. The transport versus spectroscopic T^* determination is discussed within a well defined framework.

II. METHOD AND ITS JUSTIFICATION

A. Model

The single-band Hubbard model is defined by the Hamiltonian

$$H = \sum_{\mathbf{k},\alpha=\uparrow,\downarrow} a^{\alpha\dagger}_{\mathbf{k}}(\varepsilon_{\mathbf{k}} - \mu)a^{\alpha}_{\mathbf{k}} + U\sum_{\mathbf{i}} n^{\uparrow}_{\mathbf{i}} n^{\downarrow}_{\mathbf{i}},$$
$$\varepsilon_{\mathbf{k}} = -2t(\cos k_x + \cos k_y) - 4t' \cos k_x \cos k_y - 2t''(\cos 2k_x + \cos 2k_y). \quad (1)$$

The lattice spacing a is the unit of length. Hoppings up to the third nearest neighbor are included with values $t = 250$ meV, $t' = -0.16t$, $t'' = 0.09t$. The chemical potential μ varies in a wide range, and the on-site $U = 2.5t$.

Due to strong fluctuations in two dimensions (2D), true long-range order exists only for discrete symmetry breaking. Since the model possesses a continuous $SU(2)$ spin symmetry, AF correlations are always short range. Nevertheless, a well-defined crossover temperature T^* exists that separates the short range AF from the paramagnetic phase. At least naively, the symmetry is "almost" broken in the sense that the correlator typically decreases slowly. The Gaussian

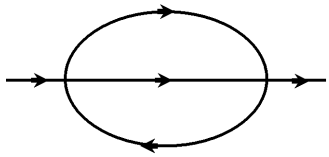

FIG. 2. The "setting sun" diagram for the self-energy that contributes to the "post-Gaussian approximation." The directed lines are Gaussian correlators, while the vertices represent the (bare) Hubbard coupling U.

covariant approximation is the simplest variational approach which may account for the (spurious) dynamical symmetry breaking. It is described in detail for bosonic and fermionic systems in Ref. [29]. In a recent paper [16] we proposed a "symmetrization" method to study strongly interacting electronic systems in the pseudogap phase. Symmetrization is achieved by integration of a one- or two-body correlator over the almost broken symmetry group. The method was tested on the benchmark models, the 1D and 2D one-band Hubbard models. Throughout the paper we use units of $\hbar = 1$, except when phenomenology is discussed.

B. Method

One starts with a solution of the Gaussian equations, paramagnetic or AF [30], ignoring the spiral ones [31], and corrects it perturbatively by adding the leading self energy correction. The method was originally proposed [32,33] in the context of bosonic theories. The paramagnetic solution of the HF equations (see Ref. [16]) for given chemical potential μ, temperature T, and couplings U, t, etc. is characterized by the density n. The inverse Green's function is

$$G_{\mathrm{HF}}^{-1} = -(\omega + i\eta_0 + e_{\mathbf{k}}), \tag{2}$$

where

$$e_{\mathbf{k}} = \varepsilon_{\mathbf{k}} - \mu_r, \tag{3}$$

with the "renormalized chemical potential"

$$\mu_r = \mu - Un/2. \tag{4}$$

The self-energy is graphically represented in Fig. 2

Its explicit form, after summation over the two loop frequencies, is

$$\Sigma(\omega, \mathbf{k}) = \frac{U^2}{4N^2} \sum_{\mathbf{l},\mathbf{m}} \frac{\left\{\tanh\left(\frac{e_{\mathbf{m}}}{2T}\right) - \tanh\left(\frac{e_{\mathbf{k}-\mathbf{l}-\mathbf{m}}}{2T}\right)\right\}\left\{\tanh\left(\frac{e_{\mathbf{l}}}{2T}\right) - \coth\left(\frac{e_{\mathbf{k}-\mathbf{l}-\mathbf{m}}-e_{\mathbf{m}}}{2T}\right)\right\}}{\omega + i\eta_0 + e_{\mathbf{l}} + e_{\mathbf{m}} - e_{\mathbf{k}-\mathbf{l}-\mathbf{m}}}, \tag{5}$$

where N is the number of the lattice points. Consequently, the post-Gaussian approximation for the (retarded) Green's function is

$$G(\omega, \mathbf{k}) = -\frac{1}{\omega + i\eta_0 + e_{\mathbf{k}} + \Sigma(\omega, \mathbf{k})}. \tag{6}$$

In the antiferromagnetic (AF) phase expressions are much more cumbersome, and it is relegated to Appendix A.

C. Phase diagram and spectral weight at intermediate coupling

The two main distinctive features, referred to as the pseudogap and the strange metal, are given in Fig. 3. A pseudogap shows up near the antinodal points below temperature T^*. It increases in the underdoped regime $p < p_{\mathrm{opt}}$ towards the Mott insulator phase and reaches values in the range $\Delta =$ 100–200 meV. Here, $p_{\mathrm{opt}} = 0.16$ is the doping where the transition temperature to superconductor is the highest. One natural explanation for this is the short range AF order, as the pseudogap regime borders the AF Mott insulator phase at very low doping. It was observed in Ref. [5] that the Fermi surface fractures into small "pockets" for dopings below the Lifshitz point p^* exactly when the pseudogap vanishes. This is well described by variants of the phenomenological RVB model (see Ref. [6]) that is derived from a Hubbard model with on site repulsion $U = 2.5t$ and hopping parameters $t =$ 250 meV, $t' = -0.16t$, $t'' = 0.09t$.

The main feature of pseudogap is observed using ARPES. The spectral weight, $A(\omega, \mathbf{k}) = -1/\pi\ \mathrm{Im}[G(\omega, \mathbf{k})]$, near the antinode measured [34] in $Bi_2Sr_2CaCu_2O_{8+p}$ (BSCCO) resembles that calculated using the post-Gaussian method. To characterize the pseudogap phase and the crossover line T^*, spectral weight, measured in numerous ARPES experiments [34,35], is calculated. In Fig. 4(a), we plot spectral weight at the Fermi level as a function of quasimomentum, with $p = 0.16$ and temperature from 100 to 280 K. One notes that the spectral weight in the antinodal region is larger than that in the nodal region by a factor of about 2.

The signature of the strange metal is linear resistivity in the temperature range 100–400 K at intermediate and relatively

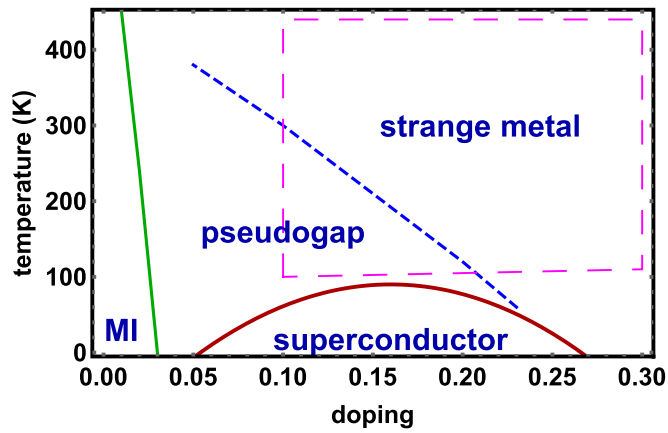

FIG. 3. Phase diagram of cuprates. The T^* line (blue) separates the pseudogap phase from the strange metal. At very low (hole) doping Mott insulator (MI) appears, while the d-wave superconductivity is observed below the dashed line.

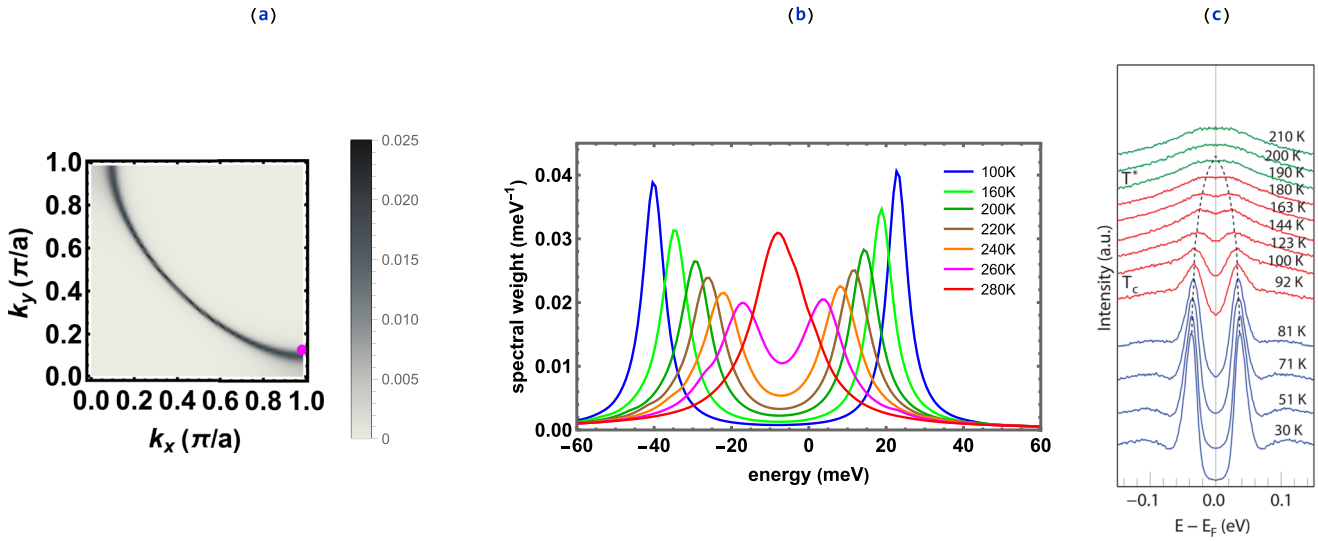

FIG. 4. (a) The zero frequency spectral weight in the first quarter of the Brillouin zone (BZ). (b) Closing the pseudogap at a point close to the Fermi surface of (a) (the pink blob) and near the antinode. Spectral weight is shown as a function of frequency. The paramagnetic phase (a single peak) is represented by $T = 280$ K. The rest are antiferromagnetic (a double peak). (c) The experiment for $Bi_2Sr_2CaCu_2O_{8+p}$ is taken from Ref. [34].

large dopings, generically above T^*. It is generally believed that the quasiparticle picture should be properly modified in this phase. Approaches such as the marginal Fermi liquid [8], quantum criticality [9], and Planckian dissipation [10], explain part of the experimental results, but typically start from Hamiltonians that are different from those used to describe the pseudogap physics. Thus each specific aspect of the normal state may be captured by a particular phenomenological model that provides a consistent description of the whole normal state (not including superconductivity) phase diagram; see Fig. 3. However, a unified theory remains evasive. Low temperature pseudogap physics may also be depicted quite well by various variational approaches.

In Fig. 4(b) the spectral weight dependence on frequency across the T^* crossover line for $p = 0.16$ is given. We choose the quasimomentum $\mathbf{k} = \pi(1, \frac{1}{8})$ close to the Fermi surface, which is indicated by the magenta blob in Fig. 4(a). Several curves for the spectral weight with temperature in the range $T = 100$–280 K are shown. The crossover T^* therefore lies in the temperature range between $T = 260$ and 280 K. The pseudogap value corresponds to the energy spacing between the two maxima. It widens as the temperature decreases. Simultaneously the peak values become higher and in the valley between them the spectral weight vanishes. These features are qualitatively consistent with ARPES [34,35] observations shown in Fig. 4(c). Spectral weight from 30 to 210 K for a slightly underdoped BSCCO sample, $T_c = 92$ K, are shown. One clearly observes, shown in Fig. 4(b), that below $T^* = 190$K a two-peak structure appears. The post-Gaussian correction modifies the HF picture by shifting T^* to a lower value and reducing the pseudogap value at low temperature. For other quasimomenta (e.g., near the nodal position given in Fig. 5) the dependence is similar and in accord with available experiments. Now, we turn to the calculation of the transport properties.

D. Scattering due to strong repulsion

The correction to the scattering rate due to interaction gives the main contribution to the resistivity in relatively clean cuprates, while the impurity scattering plays a minor role. The interaction contribution to conductivity is given by the Kubo formula (assuming the fourfold symmetry),

$$\sigma(\omega) = -\,\mathrm{Im}\,\frac{\Pi(i\omega_n)}{\omega}\bigg|_{i\omega_n=\omega+i0}, \tag{7}$$

with the current-current (Matsubara) correlator [36]

$$\Pi(i\omega_n) = e^2T\int\frac{d^2k}{(2\pi)^2}\sum_m \mathbf{v}(\mathbf{k})\cdot\mathbf{\Gamma}(\mathbf{k}; i\omega_m, i\omega_m + i\omega_n) \times G(\mathbf{k}, i\omega_m)G(\mathbf{k}, i\omega_m + i\omega_n). \tag{8}$$

Here the (unrenormalized) Fermi velocity is $v_i(\mathbf{k}) = \frac{\partial\varepsilon_\mathbf{k}}{\partial k_i}$ and $\mathbf{\Gamma}(\mathbf{k}; i\omega_m, i\omega_m + i\omega_n)$ is the current-fermion-fermion vertex function $\mathbf{\Gamma}(\mathbf{k}, \mathbf{k}+\mathbf{q}; i\omega_m, i\omega_m + i\omega_n)$ with the bosonic momentum $\boldsymbol{q} = \mathbf{0}$. Without the "vertex corrections" it is just the velocity,

$$\mathbf{\Gamma}^0(\mathbf{k}; i\nu, i\nu + i\omega_n) = \mathbf{v}(\mathbf{k}). \tag{9}$$

As will be demonstrated below, even though such a drastic simplification has been made, the strange metal behavior can still be captured correctly. The second important simplification is that we do not attempt to calculate the one-body correlator G self-consistently as in, for example, the RPA approach. In this approach, collective excitations such as paramagnon and plasmon are not included. They are not expected to participate in the explanation of the strange metal phenomenon.

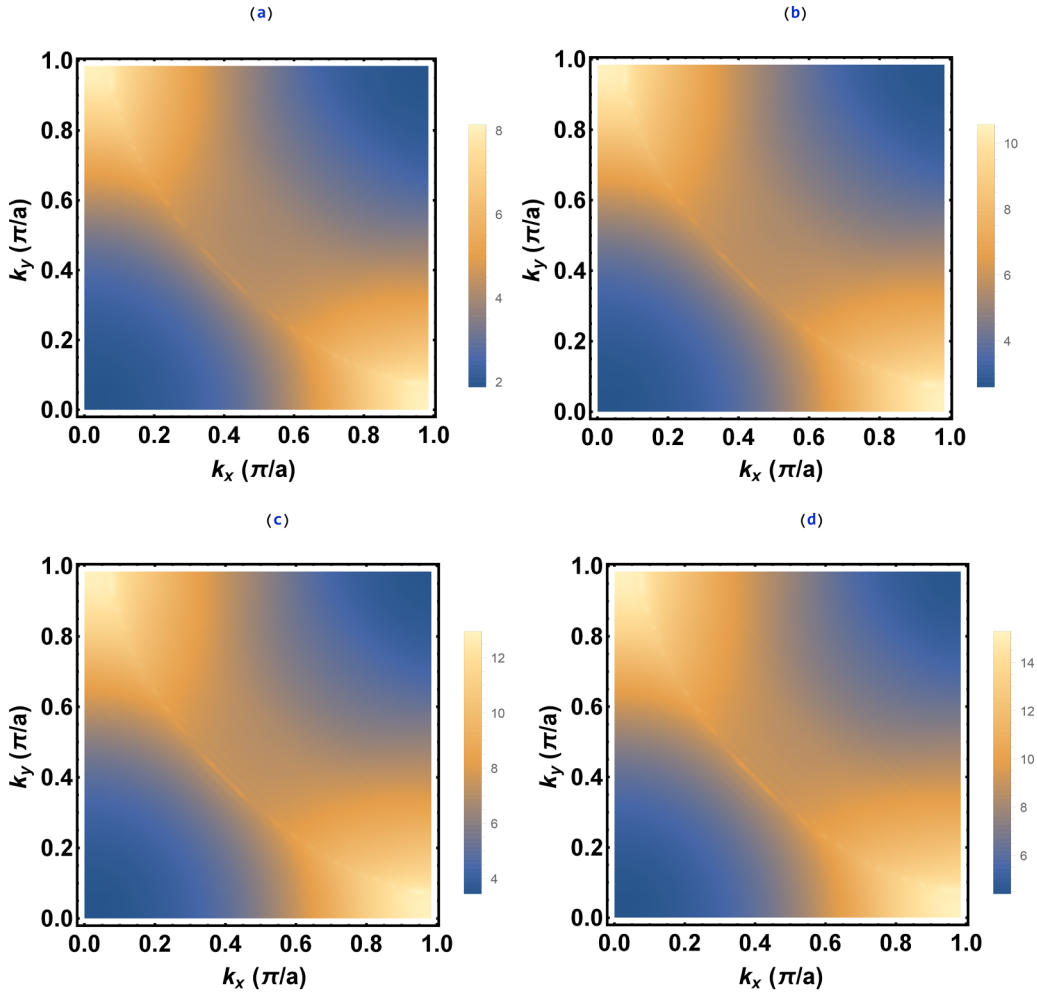

FIG. 5. The self-energy due to the Hubbard repulsion for doping $p = 0.26$. (a), (b), (c), and (d) show the imaginary part of the self-energy divided by temperature, $\mathrm{Im}[\Sigma(0, \mathrm{k})/T]$, in the first quarter of the BZ for 220, 280, 340, and 400 K, respectively.

Within this approximation the current-current correlator simplifies:

$$\Pi(i\omega_n) = e^2 T \int \frac{d^2k}{(2\pi)^2} \sum_m v^2(\mathbf{k}) G(\mathbf{k}, i\omega_m) G(\mathbf{k}, i\omega_m + i\omega_n). \tag{10}$$

Using the Lehmann representation via spectral weight A,

$$G(\mathbf{k}, i\omega_m) = \int d\nu \frac{A(k, \nu)}{i\omega_m - \nu},$$
$$G(\mathbf{k}, i\omega_m + i\omega_n) = \int d\nu \frac{A(\mathbf{k}, \nu)}{i\omega_m + i\omega_n - \nu}, \tag{11}$$

one may write the function as

$$\begin{aligned}\Pi(i\omega_n) &= e^2 T \int \frac{d^2k}{(2\pi)^2} \sum_m \int d\nu_1 d\nu_2 v^2 \\ &\quad \times (\mathbf{k}) \frac{A(\mathbf{k}, \nu_1)}{i\omega_m - \nu_1} \frac{A(\mathbf{k}, \nu_2)}{i\omega_m + i\omega_n - \nu_2} \\ &= e^2 T \int \frac{d^2k}{(2\pi)^2} \int d\nu_1 d\nu_2 v^2(\mathbf{k}) A(\mathbf{k}, \nu_1) A(\mathbf{k}, \nu_2) \\ &\quad \times \frac{f_F(\nu_1) - f_F(\nu_2)}{i\omega_n + \nu_1 - \nu_2}.\end{aligned} \tag{12}$$

Here $f_F[\varepsilon] = (1 + \exp[\varepsilon/T])^{-1}$ is the Fermi distribution. This approximation (for the *full* Green's function G) has been used to analyze the neutron scattering data with G determined by ARPES [37] and is called the generalized Lindhard function.

Performing analytic continuation for $\Pi(i\omega_n)_{i\omega_n=\omega+i0}$, one obtains the imaginary part of $\Pi(i\omega_n)_{i\omega_n=\omega+i0}$ [using the identity $\mathrm{Im}\frac{1}{\omega+i0+\nu_1-\nu_2} = -\pi\delta(\omega + \nu_1 - \nu_2)$]:

$$\begin{aligned}\mathrm{Im}\,\Pi(i\omega_n)_{i\omega_n=\omega+i0} &= -\pi e^2 T \int \frac{d^2k}{(2\pi)^2} \int d\nu_1 d\nu_2 v^2(\mathbf{k}) \\ &\quad \times A(\mathbf{k}, \nu_1) A(\mathbf{k}, \nu_2) \frac{\{f_F(\nu_1) - f_F(\nu_2)\}}{\nu_1 - \nu_2} \\ &\quad \times \delta(\omega + \nu_1 - \nu_2).\end{aligned} \tag{13}$$

Integrating over ν_2, and taking the DC limit $\omega \to 0$, one finally obtains

$$\sigma = -\frac{\pi e^2}{\hbar N} \int_{\nu=-\infty}^{\infty} f_F'(\nu) \sum_{\mathbf{k}} v(\mathbf{k})^2 A(\nu, \mathbf{k})^2. \tag{14}$$

All the frequency summations are performed exactly, so that no problematic analytic continuation is needed. Of course the range of validity of the expansion is limited by the require-

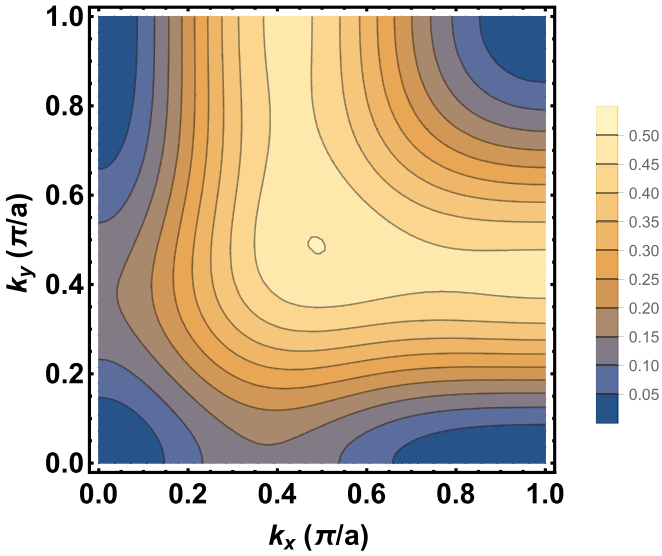

FIG. 6. The square of the Fermi velocity in the first quarter of the square lattice BZ for the parameters in the text.

ment that a higher order correction (the order is rigorously defined in Ref. [33]) around the Gaussian approximation should be smaller than the preceding ones. It is important to note that the factor

$$v(\mathbf{k})^2 = 4\{(t + 2t' \cos k_y + 4t'' \cos k_x)^2 \sin^2 k_x + (k_x \leftrightarrow k_y)\} \tag{15}$$

vanishes quadratically at the van Hove singularities Γ and M; see Fig. 6. As a consequence the antinode region and the Γ and M regions practically do not contribute to the conductivity. It turns out that the often made simplification of replacing the $f_F'[\omega]$ factor in Eq. (14) by a delta function gives erroneous results; see the next section.

III. APPLICABILITY RANGE OF THE POST-GAUSSIAN METHOD

A. General justification argument

There is no widely accepted criterion to determine the range of applicability of a nonperturbative and nonvariational approximation. The post-Gaussian method presented in the previous section uses a variational HF two-point Green's function to calculate the leading perturbative contribution to a four-point function that vanishes within the HF approximation. In particular, the Coulomb repulsion contribution to scattering rate (dissipation) is a quantity of this type. The validity of the approximation is limited by the requirement that a yet higher order correction around the Gaussian (HF) approximation (the order is rigorously defined in Ref. [32]) is smaller than the leading one. A rough criterion is that the difference between the symmetrized HF and the post-Gaussian densities is much smaller than the half-filling density. Another criterion is formulated in terms of inverse compressibility below. For a relatively small coupling $U = 2.5t$ used in this paper, the temperature applicability range is expected to extend down to the range depicted in Fig. 3 or even beyond it.

Similar views have been expressed in several investigations. In particular, the lowest order Maki-Thompson approximation was shown to be small [38]. It was shown also that the Aslamasov-Larkin terms vanish under certain conditions [39]. In addition, approximate expressions for various four-point correlators via the "exact" two-point function and (renormalized) coupling strength similar to Eq. (10) were widely used to phenomenologically relate different experimental data. The ARPES information is commonly used to determine Green's function G. In particular, the spin-spin (charge-charge) correlators measured in inelastic neutron scattering (INS) was related to Green's function in Refs. [37,40]. Electrical transport (including the Hall conductivity) was related to ARPES in Ref. [41], while the thermoelectric transport (like the Nernst effect) was studied in Ref. [42].

As mentioned above, it is difficult, however, to rely on the diagrammatic analysis (even the one based on the Bethe-Salpeter equations and Ward identities), so we would prefer to compare our calculations of the self-energy and conductivity with available Monte Carlo (MC) simulation below.

B. Comparison of compressibility with MC calculation

To establish the range of validity of the post-Gaussian approximation, we extend the high temperature comparison with MC simulation. In this subsection we compare the results of the post-Gaussian approximation for the extended Hubbard model with MC simulation in Ref. [43]. The coupling was relatively large: $U = 6t$. The dispersion relation includes up to the second nearest neighbors hopping amplitudes with $t = 250$ meV, $t' = -0.25t$, and $t'' = 0$. The chemical potential μ determines the hole doping in the range $p = 0.1$–0.3. The inverse compressibility in the high temperature range $0.2t < T < 8t$ is given in Fig. 7. The agreement is very good including the high temperature results (dashed lines) calculated analytically [44].

C. Comparison of resistivity

The DC resistivity is compared in Fig. 8. The values of resistivity and temperatures were translated to the physical units with hopping parameter $t = 250$ meV. The resistivity curves are slightly shifted (see Fig. 8) compared to the MC simulation. The case is not realistic for cuprates since the values of T^* (of order 600 at $p = 0.2$) determined from nonlinearity of $\rho(T)$ are thousands of Kelvin for low doping, much higher than the experimental observed values. Analytically demonstrated [44] linearity in the large T limit ($T \gg t$) is quite common and is not directly related to the strange metal that appears at temperatures 100–450, K which is obviously much lower than the hopping energy t. Also the resistivity is much lower than the experimental ones. However even for this coupling, the post-Gaussian approximation results are still in quantitative agreement with the MC results at high temperature $T > 1.1t \simeq 3200$ K. It may be seen that the post-Gaussian approximation is much better than the HF approximation. Even at the low temperature, the post-Gaussian approximation gives a qualitatively good description of the pseudogap phase.

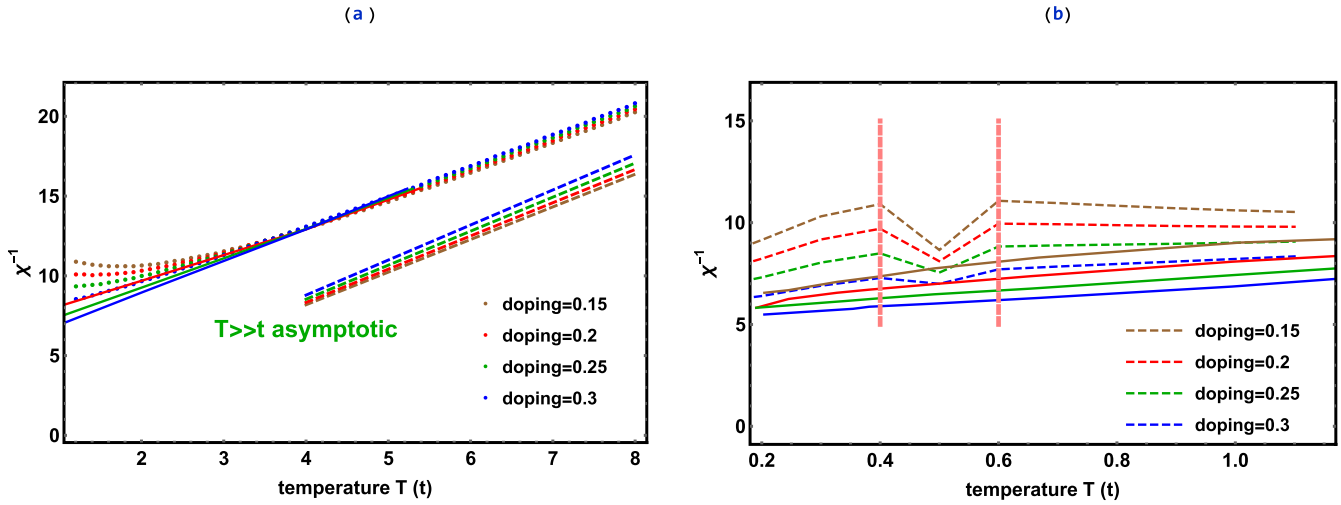

FIG. 7. The inverse compressibility of the Hubbard model at strong coupling, $U = 6t$, for various dopings. Dots are the results of the post-Gaussian approximation, while lines are the results of MC simulations. (a) The high temperature range, $T = 1.2t$–$8t$. (b) The lower temperature range, $T = 0.2t$–$1.2t$. Vertical red lines mark the intermediate range in which the post-Gaussian approximation breaks down.

IV. STRANGE METAL RESISTIVITY

A. Transport

Now let us turn to transport for the case that U is of intermediate strength. The DC resistivity (per CuO layer) is given in Fig. 9. It clearly demonstrates the linear dependence, $\rho = \rho_0 + AT$, in the strange metal region of the phase diagram. This is the main result of the present paper. The value of $A \simeq 25\ \Omega/\mathrm{K}$ (resistance per layer) at doping $p = 0.16$ are a bit higher than those found by interpolating the $La_{2-p}Sr_pCuO_4$ data of [10] to $p = 0.16$. However, as was discussed in the Introduction, the intermediate value of $U = 2.5t$ is smaller than that of $La_{2-p}Sr_pCuO_4$. We found that for higher value of U, the slope decreases. Since disorder is always present in cuprates, doping-dependent value of disorder strength $\eta_0 = \hbar/2\tau_0$ must be taken into account. We have chosen a small value of $\eta_0 = 3$ meV. Using a different value of η_0 (see Fig. B12) would increase the residual resistivity ρ_0. At higher doping the crossover to Landau liquid appears; see Fig. 9(b).

B. Scattering time

To understand qualitatively the results, we plot the integrand of the imaginary part of the self-energy (due to on-site repulsion), $\mathrm{Im}(\Sigma_k) = \hbar/2\tau_k$ at $\omega = 0$ as a function of quasimomentum in Figs. 10(a) and 10(b) for two different temperatures. For this purpose a higher doping $p = 0.26$ is considered and thus there would be no "intercept" ρ_0 in Fig. 9. Plots of the ratio $A(\mathbf{k})/T$ over the whole BZ for $T = 200$ and 400K are shown in Fig. 10 and the curves are hardly distinguishable. This demonstrate that $1/2\tau_k \propto T$. Due to the maximum of the factor $v(\mathbf{k})^2$ in Eq. (14) the most important

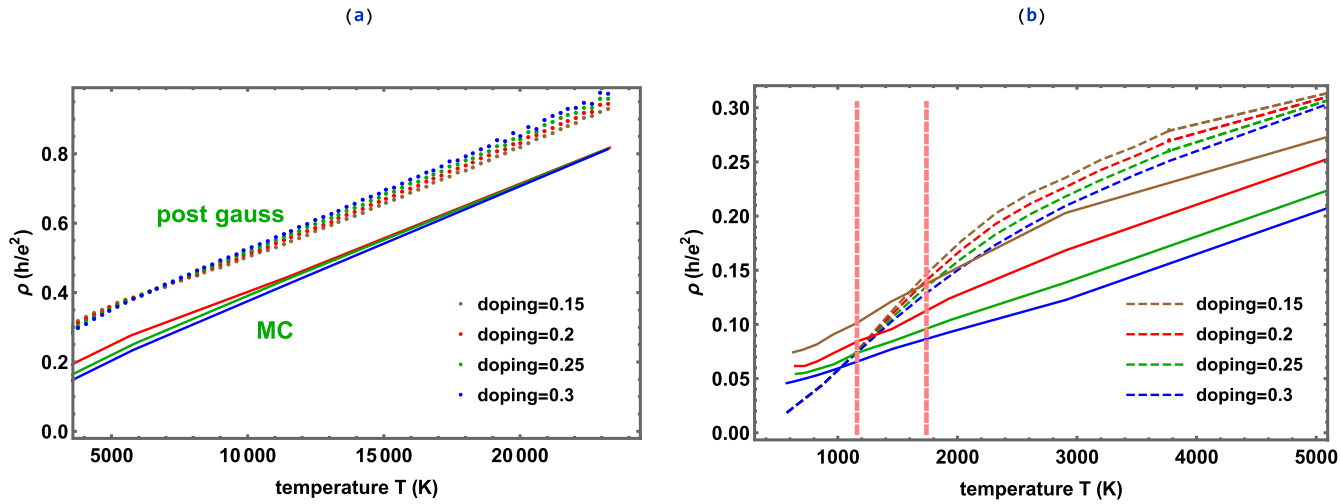

FIG. 8. Resistivity as a function of temperature of the Hubbard model at strong coupling $U = 6t$. (a) The very high temperature range, $T = 1.2t$–$8t$. (b) The lower temperature range, $T = 0.2t$–$1.4t$. Vertical red lines mark the range in which the post-Gaussian approximation breaks down.

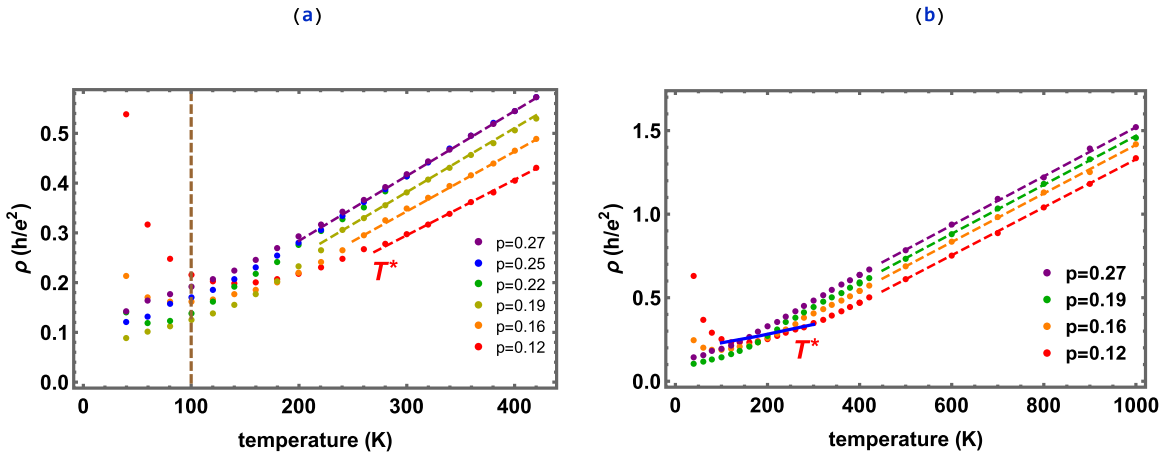

FIG. 9. Resistivity in the strange metal phase. (a) The post-Gaussian results are very accurate beyond 100 K (dashed-brown line). Dashed straight lines are interpolation. The transport determined crossover temperature is marked by T^*. (b) A larger temperature and doping range demonstrate crossover to the Landau liquid.

contribution to conductivity comes from a broad region near the nodal point. To demonstrate this, we plot the spectral weight dependence along the Γ-M line [see the pink line in Fig. 10(a)] in Fig. 10(c). The dependence on location is different for temperatures 200, 300, and 400 K. However, the three curves almost coincide when the spectral weight is divided by T, as shown in Fig. 10(d). One observes from Fig. 4(a) that the Fermi surface in this case is nearly circular.

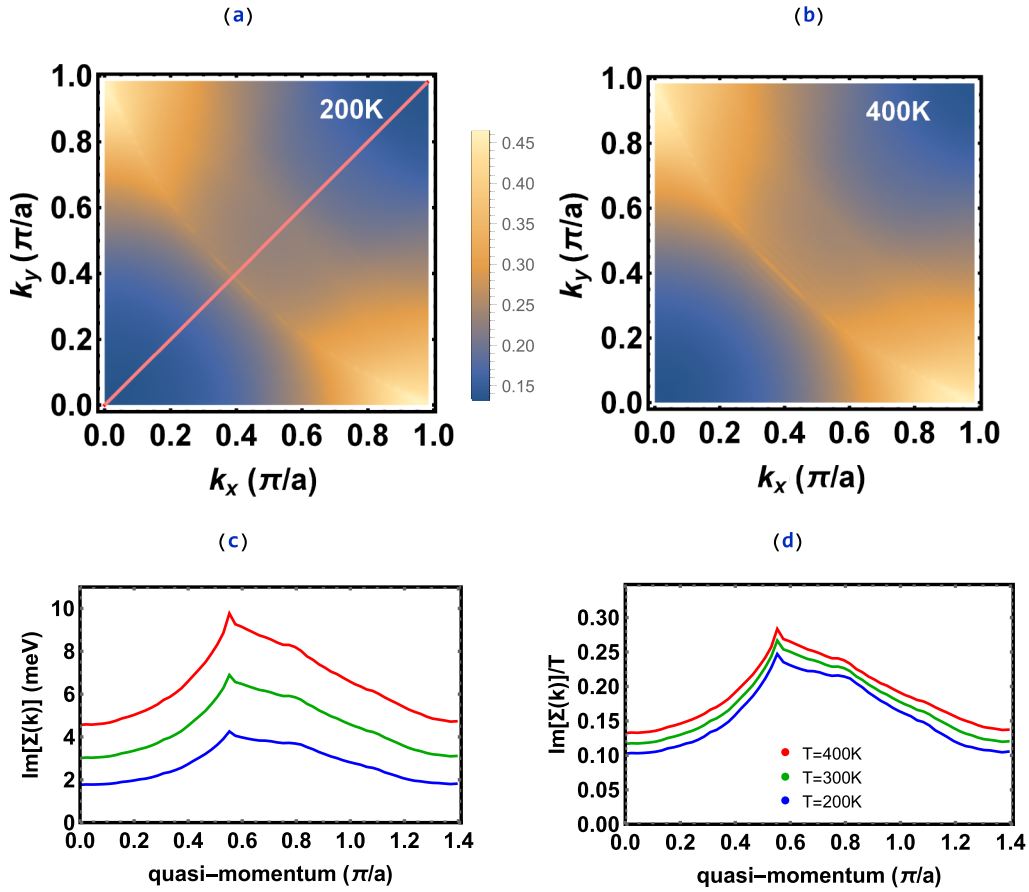

FIG. 10. (a) The self-energy due to Hubbard repulsion for doping $p = 0.26$. The imaginary part of the self-energy divided by temperature, $\mathrm{Im}[\Sigma(0, \mathrm{k})/T]$, in the first quarter of the BZ for 200 K. (b) Same for 400 K. Note the maximum on the Fermi surface [shown in Fig. 2(a)]. (c) The imaginary part of the self-energy for temperatures 200, 300, and 400 K on the Γ to M line [marked by a pink line in (a)]. (d) The imaginary part of the self-energy divided by temperature for the same temperature.

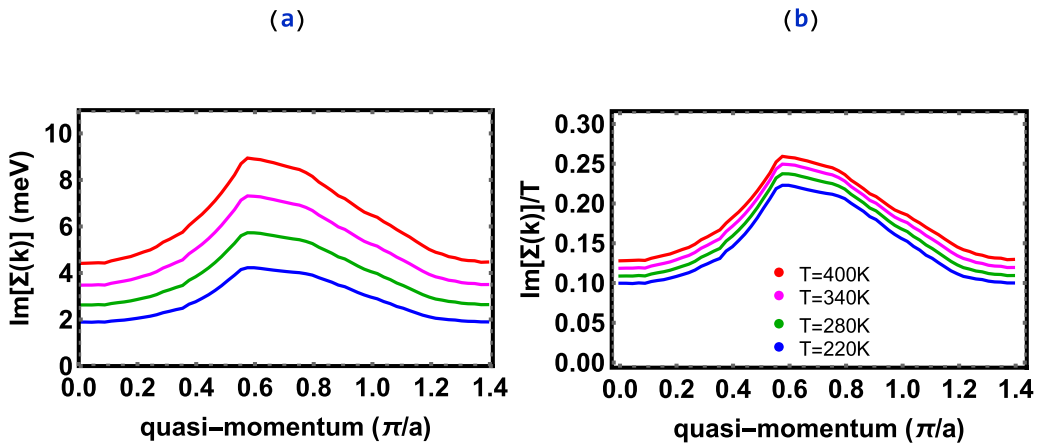

FIG. 11. (a) The imaginary part of the self-energy along the Γ-M line for various temperatures. (b) The same quantities after being scaled by temperature.

Thus the effective mass approximation can be applied to estimate the conductivity via the Drude formula $\sigma = e^2 n\tau/m^*$ with $\hbar/2\tau = \mathrm{Im}[\Sigma_{\mathrm{node}}] \simeq 0.25T$. This is close to the result in Fig. 9. Using the phenomenological (Planck) formula $A = \alpha m^*/e^2 n\hbar$ [10], one estimates $\alpha = 0.5$.

The A^2 factor in the conductivity, Eq. (14) depends crucially on the imaginary part of the self-energy $\Sigma(\omega, \mathbf{k})$ at very low frequencies [due to a strong peak of $f_F'(\omega)$]. The self-energy at zero frequency as a function of quasimomentum is given in Fig. 5. The doping $p = 0.21$ is smaller than the one ($p = 0.26$) presented in Fig. 10 of the main text, so that one can still observe the strange metal behavior of resistivity. A cut of this distribution along the Γ-M line (see Ref. [4]) is given for four temperatures in Fig. 11.

V. CONCLUSIONS

To summarize, an intermediate-coupling one-band Hubbard model can be used to describe the two most important unusual normal state features of cuprates: the pseudogap and strange metal. Both the spectroscopic and transport properties of the cuprates in the whole doping range were considered on the same footing within a relatively simple (symmetrized) post-Gaussian approximation. It is valid for intermediate couplings $U/t = 1 - 4$ in the temperature range $T = 100$–500 K. We have assumed a relatively small coupling that is independent of doping in the range 0.1–0.3. For a smaller doping, especially in the Mott insulator phase, the coupling on the effective tight binding scale increases and a different method would be required. This provides an alternative to the commonly accepted paradigm that the coupling at a significant doping should be strong enough, say $U/t > 6$, for the system to describe the strange metal. We argued (see also the description of the Lifshitz transition and fractionalization of the Fermi surface in a similar framework [24]) that to obtain phenomenologically acceptable underdoped normal state characteristics like T^*, pseudogap values, and spectral weight distribution, a large value of U is detrimental. Of course this applies only to the short range AF order interpretation of the pseudogap. Surprisingly the resistivity in the above temperature range is linear, $\rho = \rho_0 + \alpha \frac{m^*}{e^2 n\hbar} T$, with the "Planckian" coefficient $\alpha \sim 0.5$. Interestingly the spectroscopy estimate of T^* [from the vanishing of the pseudogap, Fig. 4(b), as observed in ARPES] is typically lower than that determined from resistivity (Fig. 9).

First-principles calculations for parent materials of the electron doped cuprates generally result in intermediate or even small values of the effective U [12]. The present study demonstrates that for hole doped cuprates the intermediate coupling option is viable despite the fact that most first-principles determinations for *parent materials* favor a large coupling [11]. Materials like La_2CuO_4 and $Bi_2Sr_2CuO_6$ perhaps are really strongly coupled even when doped, but higher T_c superconductors like $HgBa_2CuO_4$ and $Tl_2Ba_2CuO_6$ might belong to the intermediate coupling class when doped. The situation with two or three layered cuprates should be similar to the model adapted to include interlayer hopping.

We used a very simple approximation method [see Eq. (10)] in which the current-current correlator is given in terms of the one-body Green's function G calculated within the post-Gaussian approximation, and no vertex corrections are included. The second important simplification is that we do not attempt to calculate G self-consistently. Effectively, the Hartree-Fock correlator G_0 is just corrected by the the leading order self-energy diagram (two loop "setting-sun" diagram).

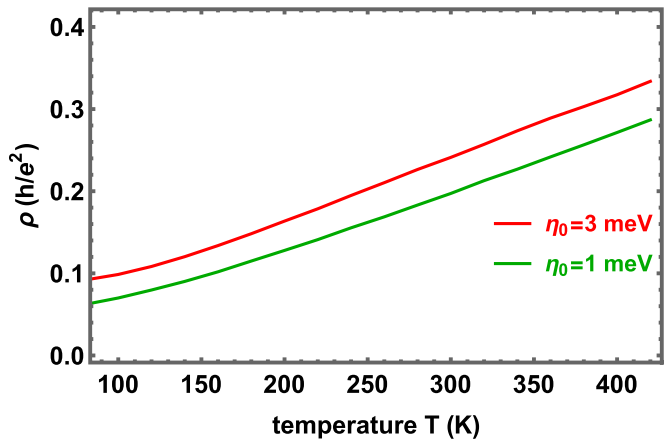

FIG. 12. Dependence of the strange metal resistivity on the disorder parameter.

This allows us to avoid doing numerical analytic continuation, which is problematic. As demonstrated above, the strange metal behavior can still be captured correctly even though such simplifications are made.

ACKNOWLEDGMENTS

The authors are very grateful to J. Wang, B. Shapiro, and Z. Sun for numerous discussions. We would also like to thank the National Center for High-performance Computing (NCHC) of National Applied Research Laboratories (NARLabs) in Taiwan for providing computational and storage resources. H.C.K. and B.R. are supported by MOST-110-2112-M-A49 012-MY2 of MOST, Taiwan. D.P.L. is supported by the National Natural Science Foundation of China (Grant No.12174006) and the High-performance Computing Platform of Peking University.

APPENDIX A: THE POST-GAUSSIAN CORRECTION TO THE (SYMMETRIZED) HARTREE-FOCK APPROXIMATION

1. Self-energy in the AF phase

The AF solution of the HF equations, see Ref. [16], for given chemical potential μ, temperature T and couplings U, t, etc. is characterized by the density n and pseudogap Δ. The inverse Green's function is a matrix in the sublattice space,

$$G^{-1}_{s,\mathrm{HF}} = \begin{pmatrix} \omega + i\eta_0 + e'_{\mathbf{k}} + (-1)^s\Delta & h_{\mathbf{k}} \\ h^*_{\mathbf{k}} & \omega + i\eta_0 + e'_{\mathbf{k}} + (-1)^s\Delta \end{pmatrix}, \tag{A1}$$

where

$$\begin{aligned} e'_{\mathbf{k}} &= -4t'\cos(2\pi k_1/N_x)\cos[2\pi(k_1-k_y)/N_x] - 2t''\{\cos(4\pi k_1/N_x) + \cos[4\pi(k_1-k_y)/N_x]\} - \mu_r, \\ x^2_{\mathbf{k}} &= \Delta^2 + \{2t[\cos(2\pi k_1/N_x) + \cos(2\pi(k_1-k_y)/N_x)]\}^2, \\ h_{\mathbf{k}} &= t(1 + e^{i2\pi(2k_1/N_x)} + e^{i2\pi(k_y/N_x)} + e^{i2\pi(2k_1-k_y)/N_x}). \end{aligned} \tag{A2}$$

The self-energy is also a spin dependent matrix in the sub-lattice space. $G^{-1} = G^{-1}_{HF} - \Sigma$, with the diagonal components

$$\Sigma^{AA}_s(\omega,\mathbf{k}) = \Sigma^{BB}_s(\omega,\mathbf{k}) = \frac{4U^2}{N^2}\sum_{\mathbf{p},\mathbf{q}} S_{\mathrm{diag}}(\omega, x_{\mathbf{p}}, x_{\mathbf{q}}, x_{\mathbf{p+q-k}}, -e'_{\mathbf{p}}, -e'_{\mathbf{q}}, -e'_{\mathbf{p+q-k}}, (-1)^{s+1}\Delta) \tag{A3}$$

and of-diagonal ones

$$\Sigma^{AB}_s(\omega,\mathbf{k}) = \frac{4U^2t^3}{N^2}\sum_{\mathbf{p},\mathbf{q}} \phi_{\mathbf{p}}\phi_{\mathbf{q}}\phi^*_{\mathbf{p+q-k}} S_{\mathrm{off}}(\omega, x_{\mathbf{p}}, x_{\mathbf{q}}, x_{\mathbf{p+q-k}}, -e'_{\mathbf{p}}, -e'_{\mathbf{q}}, -e'_{\mathbf{p+q-k}}), \tag{A4}$$

$$\Sigma^{BA}_s(\omega,\mathbf{k}) = \frac{4U^2t^3}{N^2}\sum_{\mathbf{p},\mathbf{q}} \phi^*_{\mathbf{p}}\phi^*_{\mathbf{q}}\phi_{\mathbf{p+q-k}} S_{\mathrm{off}}(\omega, x_{\mathbf{p}}, x_{\mathbf{q}}, x_{\mathbf{p+q-k}}, -e'_{\mathbf{p}}, -e'_{\mathbf{q}}, -e'_{\mathbf{p+q-k}}).$$

The corresponding functions are

$$\begin{aligned} S_{\mathrm{off}}(\omega,a,b,c,\alpha,\beta,\gamma) = \frac{1}{16abc}\Bigg[& c\tanh\left[\frac{-b+\beta}{2T}\right]\left\{-\frac{\tanh\left[\frac{-a+\alpha}{2T}\right]}{(a+b+\omega-\alpha-\beta+\gamma)^2-c^2} + \frac{\tanh\left[\frac{a+\alpha}{2T}\right]}{(a-b-\omega+\alpha+\beta-\gamma)^2-c^2}\right\} \\ & + c\tanh\left[\frac{b+\beta}{2T}\right]\left\{\frac{\tanh\left[\frac{-a+\alpha}{2T}\right]}{(a-b+\omega-\alpha-\beta+\gamma)^2-c^2} - \frac{\tanh\left[\frac{a+\alpha}{2T}\right]}{(a+b-\omega+\alpha+\beta-\gamma)^2-c^2}\right\} \\ & + b\tanh\left[\frac{-c+\gamma}{2T}\right]\left\{-\frac{\tanh\left[\frac{-a+\alpha}{2T}\right]}{(a-c+\omega-\alpha-\beta+\gamma)^2-b^2} + \frac{\tanh\left[\frac{a+\alpha}{2T}\right]}{(-a-c+\omega-\alpha-\beta+\gamma)^2-b^2}\right\} \\ & + b\tanh\left[\frac{c+\gamma}{2T}\right]\left\{\frac{\tanh\left[\frac{-a+\alpha}{2T}\right]}{(a+c+\omega-\alpha-\beta+\gamma)^2-b^2} - \frac{\tanh\left[\frac{a+\alpha}{2T}\right]}{(-a+c+\omega-\alpha-\beta+\gamma)^2-b^2}\right\} \\ & + a\coth\left[\frac{-b+c+\beta-\gamma}{2T}\right]\frac{\tanh\left[\frac{-c+\gamma}{2T}\right]-\tanh\left[\frac{-b+\beta}{2T}\right]}{(-b+c-\omega+\alpha+\beta-\gamma)^2-a^2} \\ & + a\coth\left[\frac{b+c-\beta+\gamma}{2T}\right]\frac{\tanh\left[\frac{-c+\gamma}{2T}\right]-\tanh\left[\frac{c+\gamma}{2T}\right]}{(b+c+\omega-\alpha-\beta+\gamma)^2-a^2} \end{aligned}$$

$$+a\coth\left[\frac{b+c+\beta-\gamma}{2T}\right]\frac{\tanh\left[\frac{-b+\beta}{2T}\right]-\tanh\left[\frac{b+\beta}{2T}\right]}{(b+c-\omega+\alpha+\beta-\gamma)^2-a^2}$$
$$+a\coth\left[\frac{-b+c-\beta+\gamma}{2T}\right]\frac{\tanh\left[\frac{c+\gamma}{2T}\right]-\tanh\left[\frac{b+\beta}{2T}\right]}{(b-c-\omega+\alpha+\beta-\gamma)^2-a^2}\Bigg]. \tag{A5}$$

In the last four terms, l'Hopital's rule must be used when the argument of hyperbolic cotangent is vanishing.

The diagonal self-energy function has the following form:

$$S_{\rm diag}(\omega,a,b,c,\alpha,\beta,\gamma,\Delta)=\frac{1}{16abc}\sum_{i=1}^{8}s_i, \tag{A6}$$

where

$$s_1=c(a+\Delta)\tanh\left[\frac{-a+\alpha}{2T}\right]\Bigg\{-\tanh\left[\frac{-b+\beta}{2T}\right]\frac{(-b+\Delta)(a+b+\omega-\alpha-\beta+\gamma-\Delta)}{(a+b+\omega-\alpha-\beta+\gamma)^2-c^2}$$
$$+\tanh\left[\frac{b+\beta}{2T}\right]\frac{(b+\Delta)(a-b+\omega-\alpha-\beta+\gamma-\Delta)}{(a-b+\omega-\alpha-\beta+\gamma)^2-c^2}\Bigg\}, \tag{A7}$$
$$s_2=c(a-\Delta)\tanh\left[\frac{a+\alpha}{2T}\right]\Bigg\{\tanh\left[\frac{-b+\beta}{2T}\right]\frac{(-b+\Delta)(a-b-\omega+\alpha+\beta-\gamma+\Delta)}{(a-b-\omega+\alpha+\beta-\gamma)^2-c^2}$$
$$-\tanh\left[\frac{b+\beta}{2T}\right]\frac{(b+\Delta)(a+b-\omega+\alpha+\beta-\gamma+\Delta)}{(a+b-\omega+\alpha+\beta-\gamma)^2-c^2}\Bigg\},$$
$$s_3=b(a+\Delta)\tanh\left[\frac{-a+\alpha}{2T}\right]\Bigg\{\tanh\left[\frac{-c+\gamma}{2T}\right]\frac{(-c+\Delta)(a-c+\omega-\alpha-\beta+\gamma+\Delta)}{(a-c+\omega-\alpha-\beta+\gamma)^2-b^2}$$
$$-\tanh\left[\frac{c+\gamma}{2T}\right]\frac{(c+\Delta)(a+c+\omega-\alpha-\beta+\gamma+\Delta)}{(a+c+\omega-\alpha-\beta+\gamma)^2-b^2}\Bigg\},$$
$$s_4=b(a-\Delta)\tanh\left[\frac{a+\alpha}{2T}\right]\Bigg\{\tanh\left[\frac{-c+\gamma}{2T}\right]\frac{(-c+\Delta)(-a-c+\omega-\alpha-\beta+\gamma+\Delta)}{(-a-c+\omega-\alpha-\beta+\gamma)^2-b^2}$$
$$-\tanh\left[\frac{c+\gamma}{2T}\right]\frac{(c+\Delta)(-a+c+\omega-\alpha-\beta+\gamma+\Delta)}{(-a+c+\omega-\alpha-\beta+\gamma)^2-b^2}\Bigg\}, \tag{A8}$$

$$s_5=-a(c-\Delta)(-b+\Delta)\coth\left[\frac{b-c-\beta+\gamma}{2T}\right]\left(\tanh\left[\frac{-c+\gamma}{2T}\right]-\tanh\left[\frac{-b+\beta}{2T}\right]\right)\frac{-b+c-\omega+\alpha+\beta-\gamma+\Delta}{(-b+c-\omega+\alpha+\beta-\gamma)^2-a^2},$$
$$s_6=a(b-\Delta)(c+\Delta)\coth\left[\frac{b+c-\beta+\gamma}{2T}\right]\left(\tanh\left[\frac{c+\gamma}{2T}\right]-\tanh\left[\frac{-b+\beta}{2T}\right]\right)\frac{b+c+\omega-\alpha-\beta+\gamma-\Delta}{(b+c+\omega-\alpha-\beta+\gamma)^2-a^2},$$
$$s_7=a(c-\Delta)(b+\Delta)\coth\left[\frac{b+c+\beta-\gamma}{2T}\right]\left(\tanh\left[\frac{-c+\gamma}{2T}\right]-\tanh\left[\frac{b+\beta}{2T}\right]\right)\frac{b+c-\omega+\alpha+\beta-\gamma+\Delta}{(b+c-\omega+\alpha+\beta-\gamma)^2-a^2},$$
$$s_8=a(c+\Delta)(b+\Delta)\coth\left[\frac{-b+c-\beta+\gamma}{2T}\right]\left(\tanh\left[\frac{b+\beta}{2T}\right]-\tanh\left[\frac{c+\gamma}{2T}\right]\right)\frac{b-c-\omega+\alpha+\beta-\gamma+\Delta}{(b-c-\omega+\alpha+\beta-\gamma)^2-a^2}.$$

Mathematica and C++ expressions for the self-energy (including the functions) are available online [45].

2. Symmetrization in the short range AF phase

The simplest variational approach in which the (spurious) dynamical symmetry breaking may be described is the Gaussian covariant approximation. It is explained in detail for bosonic and fermionic systems in Ref. [29] . In a recent paper, Ref. [16], we proposed a "symmetrization" method to study strongly interacting electronic systems in the pseudogap phase. Here we outline the main features. For the "almost broken" $SU(2)$ spin rotations of the electron field, $\psi_{\mathbf{i}}^{\alpha}\to U^{\alpha\beta}\psi_{\mathbf{i}}^{\beta}$, the one body Green's function takes the form

$$G_{\mathbf{i}-\mathbf{j}}^{\alpha\beta}=\langle\psi_{\mathbf{i}}^{*\alpha}\psi_{\mathbf{j}}^{\beta}\rangle\to\int_U U^{*\alpha\sigma}U^{\beta\rho}\langle\psi_{\mathbf{i}}^{*\sigma}\psi_{\mathbf{j}}^{\rho}\rangle. \tag{A9}$$

The (Ter Haar) integration over the group can be simplified in the $SU(2t)$ case tond

$$[G^{\alpha\beta}]^{\rm sym} = \frac{1}{2}\delta^{\alpha\beta}(G^{\uparrow\uparrow} + G^{\downarrow\downarrow}). \tag{A10}$$

The method was tested on the benchmark models, the 1D and 2D one band Hubbard models for which exact diagonalization or MC simulations have been performed.

3. Comparative contributions of the singlet ("charge"), the triplet ("spin"), and the particle-particle channels

First let us separate the diagram contributions to the self-energy into the particle-hole and the particle-particle channels, $\Sigma^{\rm ph} + \Sigma^{\rm pp}$:

$$\Sigma(\omega, \mathbf{k}) = \frac{1}{TN}\sum_{\nu,\mathbf{q}}\{G(\omega - \nu, \mathbf{k} - \mathbf{q})V^{\rm ph}(\nu, \mathbf{q}) + G(-\omega + \nu, -k + q)V^{\rm pp}(\nu, \mathbf{q})\}. \tag{A11}$$

The susceptibility part for the particle-particle channel is

$$V^{\rm pp}(\nu, \mathbf{q}) = -\frac{U^2}{3}\chi^{\rm pp}(\nu, \mathbf{q}) = -\frac{U^2}{3NT}\sum_{\sigma,\mathbf{p}} G(\sigma, \mathbf{p})G(\nu - \sigma, \mathbf{q} - \mathbf{p}). \tag{A12}$$

Meanwhile, the particle-hole part can be further divided into the singlet ("charge") and the triplet ("spin"), $V^{\rm ch} + V^{\rm spin}$:

$$V^{\rm ch}(\nu, \mathbf{q}) = \frac{1}{6}U^2\chi^{\rm ph}(\nu, \mathbf{q}), \tag{A13}$$

$$V^{\rm spin}(\nu, \mathbf{q}) = \frac{1}{2}U^2\chi^{\rm ph}(\nu, \mathbf{q}).$$

Here the susceptibility is

$$\chi^{\rm ph}(\nu, \mathbf{q}) = -\frac{1}{TN}\sum_{\sigma,\mathbf{p}} G(\sigma, \mathbf{p})G(\nu + \sigma, \mathbf{q} + \mathbf{p}). \tag{A14}$$

The "fish" integrals, involving two Green's functions, for the particle-particle and the particle-hole contributions in the paramagnetic phase, are the same. The three contributions are therefore proportional to on another, with the dominant one being the spin channel.

APPENDIX B: CONDUCTIVITY DEPENDENCE ON DISORDER

Disorder on the microscopic level is represented by the parameter $\eta_0 = \hbar/2\tau_0$. In Fig. 12 two values of this parameter are compared. As expected, the resistivities for a larger value $\eta_0 = 3$ meV and a very small value $\eta_0 = 1$ meV differ by a shift.

[1] S Hüfner, M. A. Hossain, A. Damascelli, and G. A. Sawatzky, Rep. Prog. Phys. **71**, 062501 (2008); J. P. Carbotte, T. Timusk, and J. Hwang, *ibid.* **74**, 066501 (2011).

[2] B. Keimer, S. A. Kivelson, M. R. Norman, S. Uchida, and J. Zaanen, Nature (London) **518**, 179 (2015).

[3] J. L. Tallon and J. W. Loram, Physica C **349**, 53 (2001); J. L. Tallon, J. G. Storey, J. R. Cooper, and J. W. Loram, Phys. Rev. B **101**, 174512 (2020).

[4] I. M. Vishik *et al.*, Proc. Natl. Acad. Sci. USA **109**, 18332 (2012); M. Hashimoto, I. M. Vishik, R.-H. He, T. P. Devereaux, and Z.-X. Shen, Nat. Phys. **10**, 483 (2014)

[5] S. Benhabib, A. Sacuto, M. Civelli, I. Paul, M. Cazayous, Y. Gallais, M.-A. Méasson, R. D. Zhong, J. Schneeloch, G. D. Gu, D. Colson, and A. Forget, Phys. Rev. Lett. **114**, 147001 (2015).

[6] K.-Y. Yang, T. M. Rice, and F. C. Zhang, Phys. Rev. B **73**, 174501 (2006); T. M. Rice, K.-Y. Yang, and F. C. Zhang, Rep. Prog. Phys. **75**, 016502 (2012).

[7] J. Reiss, D. Rohe, and W. Metzner, Phys. Rev. B **75**, 075110 (2007); Y. Yamaji and M. Imada, *ibid.* **83**, 214522 (2011).

[8] C. M. Varma, Phys. Rev. B **55**, 14554 (1997); Rev. Mod. Phys. **92**, 031001 (2020).

[9] P. Coleman and A. J. Schofeld, Nature **433**, 226 (2005).

[10] A. Legros, S. Benhabib, W. Tabis, F. Laliberté, M. Dion, M. Lizaire, B. Vignolle, D. Vignolles, H. Raffy, Z. Z. Li, P. Auban-Senzier, N. Doiron-Leyraud, P. Fournier, D. Colson, L. Taillefer, and C. Proust, Nat. Phys. **15**, 142 (2019).

[11] F. Nilsson, K. Karlsson, and F. Aryasetiawan, Phys. Rev. B **99**, 075135 (2019).

[12] S. W. Jang, H. Sakakibara, H. Kino, T. Kotani, K. Kuroki, and M. J. Han, Sci. Rep. **6**, 33397 (2016).

[13] J. Hea, C. R. Rotundua, M. S. Scheurerd, Y. Hea, M. Hashimoto, K.-J. Xu, Y. Wang, E. W. Huang, T. Jia, S. Chen, B. Moritz, D. Lue, Y. S. Lee, T. P. Devereaux, and Z.-X. Shen, Proc. Natl. Acad. Sci. U.S.A. **116**, 3449 (2019).

[14] J. W. Furness, Y. Zhang, C. Lane, I. Gianina Buda, B. Barbiellini, R. S. Markiewicz, A. Bansil, J. Sun, Commun. Phys. **1**, 11 (2018).
[15] K. Borejsza and N. Dupuis, Europhys. Lett. **63**, 722 (2003).
[16] B. Rosenstein, D. Li, T. X. Ma, and H. C. Kao, Phys. Rev. B **100**, 125140 (2019).
[17] A. Reymbaut, S. Bergeron, R. Garioud, M. Thenault, M. Charlebois, P. Semon, and A.-M. S. Tremblay, Phys. Rev. Res. **1**, 023015 (2019).
[18] R. S. Markiewicz, I. G. Buda, P. Mistark, C. Lane, and A. Bansil, Sci. Rep. **7**, 44008 (2017).
[19] B.-X. Zheng, C.-M. Chung, P. Corboz, G. Ehlers, M.-P. Qin, R. M. Noack, H. Shi, S. R. White, S. Zhang, and G. K.-L. Chan, Science **358**, 1155 (2017); K. Ido, T. Ohgoe, and M. Imada, Phys. Rev. B **97**, 045138 (2018).
[20] H.-C. Jiang and T. P. Devereaux, Science **365**, 1424 (2019); M. Qin, C.-M. Chung, H. Shi, E. Vitali, C. Hubig, U. Schollwöck, S. R. White, and S. Zhang, Phys. Rev. X **10**, 031016 (2020).
[21] R. E. I. Sherman, Phys. Scr. **96**, 095804 (2021).
[22] S. Raghu, S. A. Kivelson, and D. J. Scalapino, Phys. Rev. B **81**, 224505 (2010).
[23] F. Šimkovic, Y. Deng, and E. Kozik, Phys. Rev. B **104**, L020507 (2021).
[24] B. Rosenstein and B. Ya. Shapiro, J. Phys. Commun. **5**, 055013 (2021).
[25] S. Dzhumanov, arXiv:1912.12407, and references therein.
[26] S.-D. Chen, M. Hashimoto, Y. He, D. Song, K.-J. Xu, J.-F. He, T. P. Devereaux, H. Eisaki, D.-H. Lu, J. Zaanen, and Z.-X. Shen, Science **366**, 1099 (2019).
[27] C. Putzke, S. Benhabib, W. Tabis, J. Ayres, Z. Wang, L. Malone, S. Licciardello, J. Lu, T. Kondo, T. Takeuchi, N. E. Hussey, J. R. Cooper, and A. Carrington, Nat. Phys. **17**, 826 (2021).
[28] M. K. Chan, C. J. Dorow, L. Mangin-Thro, Y. Tang, Y. Ge, M. J. Veit, G. Yu, X. Zhao, A. D. Christianson, J. T. Park, Y. Sidis, P. Steffens, D. L. Abernathy, P. Bourges, and M. Greven, Nat. Commun. **7**, 10819 (2016).
[29] J. F. Wang, D. P. Li, H. C. Kao, and B. Rosenstein, Ann. Phys. (NY) **380**, 228 (2017); B. Rosenstein and A. Kovner, Phys. Rev. D **40**, 523 (1989); B. Rosenstein and D. Li, Phys. Rev. B **98**, 155126 (2018).
[30] J. E. Hirsch, Phys. Rev. B **31**, 4403 (1985); H. Q. Lin and J. E. Hirsch, *ibid.* **35**, 3359 (1987).
[31] M. A. Timirgazin, P. A. Igoshev, A. K. Arzhnikov. V. Yu. Irkhin, J. Low Temp. Phys. **185**, 651 (2016).
[32] G. J. Ruggeri and D. J. Thouless, J. Phys. F: Met. Phys. **6**, 2063 (1976).
[33] B. Rosenstein and D. Li, Rev. Mod. Phys. **82**, 109 (2010).
[34] I. M. Vishik, Rep. Prog. Phys. **81**, 062501 (2018).
[35] I. M. Vishik, N. Barisic, M. K. Chan, Y. Li, D. D. Xia, G. Yu, X. Zhao, W. S. Lee, W. Meevasana, T. P. Devereaux, M. Greven, and Z.-X. Shen, Phys. Rev. B **89**, 195141 (2014); Y.-G. Zhong, J.-Y. Guan, X. Shi, J. Zhao, Z.-C. Rao, C.-Y. Tang, H.-J. Liu, Z. Y. Weng, Z. Q. Wang, G. D. Gu, T. Qian, Y.-J. Sun, and H. Ding, *ibid.* **98**, 140507(R) (2018).
[36] G. D. Mahan, *Many-Particle Physics*, 3rd ed. (Springer, New York, 2000).
[37] D. S. Inosov, S. V. Borisenko, I. Eremin, A. A. Kordyuk, V. B. Zabolotnyy, J. Geck, A. Koitzsch, J. Fink, M. Knupfer, and B. Buchner, Physica C **460-462**, 939 (2007).
[38] S. Ray and T. Das, arXiv:1703.06280.
[39] S. A. Hartnoll, D. M. Hofman, M. A. Metlitski, and S. Sachdev, Phys. Rev. B **84**, 125115 (2011).
[40] T. Dahm and L. Tewordt, Phys. Rev. B **52**, 1297 (1995); M. Eschrig and M. R. Norman, Phys. Rev. Lett. **89**, 277005 (2002); see review by D. S. Inosov, Ph.D. thesis, TU Dresden, 2008.
[41] P. Voruganti, A. Golubentsev, and S. John, Phys. Rev. B **45**, 13945 (1992); J. G. Storey, Europhys. Lett. **113**, 27003 (2016); J. Mitscherling and W. Metzner, Phys. Rev. B **98**, 195126 (2018).
[42] A. Levchenko, M. R. Norman, and A. A. Varlamov, Phys. Rev. B **83**, 020506(R) (2011).
[43] E. W. Huang, R. Sheppard, B. Moritz, and T. P. Devereaux, Science **366**, 987 (2019).
[44] J. Kokalj, Phys. Rev. B **95**, 041110(R) (2017); C. H. Mousatov, I. Esterlis, and S. A. Hartnoll, Phys. Rev. Lett. **122**, 186601 (2019).
[45] https://phy.ntnu.edu.tw/~hckao/. There are five relevant files: List.h, function1.h, main.cpp, stdafx.cpp, and postgaussian2D.nb.